



# Explaining darker deep convective clouds over the western Pacific than over tropical continental convective regions

B.-J. Sohn, M.-J. Choi, and J. Ryu

School of Earth and Environmental Sciences, Seoul National University, Seoul, 151-747, Korea

Correspondence to: B.-J. Sohn (sohn@snu.ac.kr)

Received: 14 November 2014 – Published in Atmos. Meas. Tech. Discuss.: 4 March 2015

Revised: 10 October 2015 – Accepted: 13 October 2015 – Published: 2 November 2015

**Abstract.** This study attempted to explain why deep convective clouds (DCCs) over the western Pacific are generally darker than those found over tropical African and South American land regions. The western Pacific domain was further divided into its land and ocean regions to deduce the general differences in DCC characteristics between convectively active tropical land and ocean regions. DCC in this study is defined as a single-layer cloud whose thickness is greater than 15 km, and it is determined from CloudSat-measured reflectivity profiles. Corresponding MODIS-measured reflectivities at  $0.645\ \mu\text{m}$  were examined, along with the analysis of cloud products from Cloud Aerosol Lidar Infrared Pathfinder Satellite Observation (CALIPSO) measurements.

From an analysis of the four January months of 2007–2010, a distinct difference in ice water path (IWP) between the ocean region of the western Pacific and the three tropical land regions was revealed. Distinct differences in the effective radius between land and ocean were also found. The findings lead to a conclusion that smaller IWP over the western Pacific ocean region than over the tropical land regions, which should be caused by different cloud microphysics between land and ocean, is the main cause of smaller reflectivity there.

## 1 Introduction

Deep convective clouds (DCCs) associated with strong convection play an important role in the global climate because DCCs can alter the radiation balance not only due to changes in solar reflectivity or infrared emission level but also due to changes in water vapor and hydrometeor profiles associated with deep convection. DCCs are known to be poten-

tially important in the radiation balance (e.g., Soden and Fu, 1995; Aumann et al., 2007). DCCs over the tropics can supply moisture from the lower troposphere to the upper troposphere, enhancing the water-vapor greenhouse effect (Soden and Fu, 1995; Sohn and Schmetz, 2004; Chung et al., 2007; Sohn et al., 2008). Furthermore, DCCs can be used as calibration targets from which satellite-borne solar channels can be calibrated (Sohn et al., 2009; Ham and Sohn, 2010; Doelling et al., 2013; Kim et al., 2014). Thus, it is of interest to examine the optical and physical properties of DCCs to attain a better understanding of their impact on the radiation balance and for better parameterization of their optical properties for radiative transfer simulations.

A recent study by Doelling et al. (2013), based on an analysis of Moderate Resolution Imaging Spectroradiometer (MODIS) solar channel measurements, reported that DCCs over the tropical western Pacific have lower reflectivity (or are darker) than DCCs over continental tropical regions such as Africa and South America. This phenomenon is quite interesting and an immediate attempt to explain the reason for it may be related to different cloud microphysics between land and ocean. The difference in the diurnal cycle of convection and the vertical structure of DCCs between the oceanic western Pacific and tropical South American or African land regions has been well documented (e.g., Liu and Zipser, 2005; Nesbitt et al., 2006; Zipser et al., 2006; Liu et al., 2007). Most of these results are based on Tropical Rainfall Measuring Mission (TRMM) measurements. However, considering that TRMM radar signals reflect microwave interactions with raindrops and precipitation-size ice particles, these analyses may be insufficient for explaining the difference in cloud reflectivity. Scattered solar radiation caused by

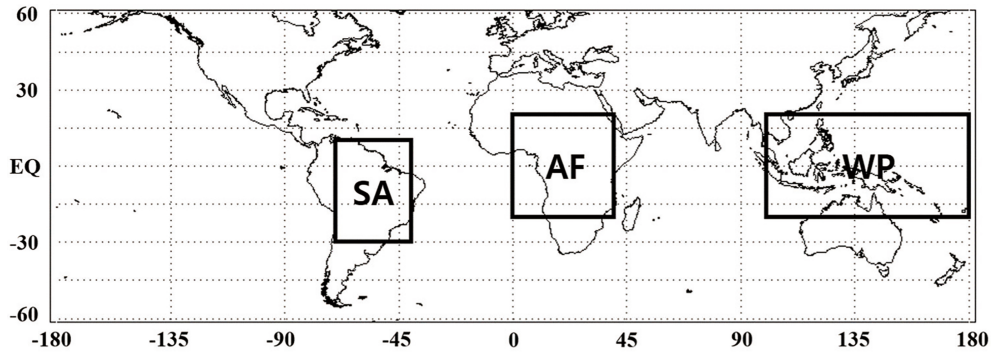


**Figure 1.** Analysis domains used in this study. SA, AF, and WP represent South American, Central African, and the western Pacific domains, respectively. The western Pacific domain is further divided into its land (WP-land) and ocean area (WP-ocean) in this study.

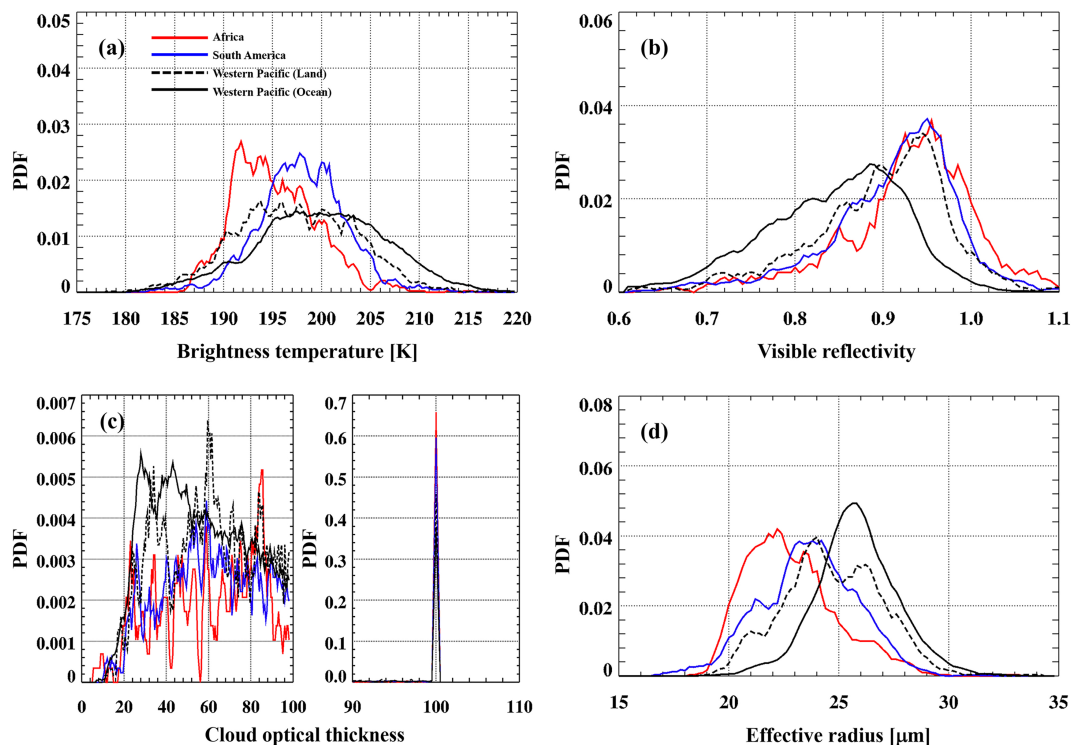


**Figure 2.** Distributions of PDFs of (a) brightness temperature at  $11\ \mu\text{m}$ , (b) reflectivity at  $0.645\ \mu\text{m}$ , and (c) cloud optical thickness; (d) effective radius from MODIS products. All data are from MODIS measurements and associated products. The red, blue, yellow, and black solid lines represent DCCs observed over African, South American, WP-land, and WP-ocean domains, respectively.

cloud droplets and ice particles should be considered to completely understand the cause of such a difference.

In this study, with the goal of understanding why DCCs over the western Pacific show generally lower reflectivity in comparison with those over tropical African and South American regions, regional differences in optical properties of DCCs are examined using CloudSat Cloud Profile Radar (CPR) and Cloud Aerosol Lidar Infrared Pathfinder Satellite Observation (CALIPSO) measurements. From an intercomparison of the vertical structures of DCC optical properties,

important elements causing regional differences in DCC reflectivity are identified. Then, we address the issue of how the obtained results are relevant for the possible use of DCCs as calibration targets from which satellite-borne solar channels can be calibrated. The results obtained from this study will lead to a better understanding of the role of tropical DCCs in influencing radiation budgets and climate feedback and may also improve the performance in the use of DCC targets for solar channel calibration.

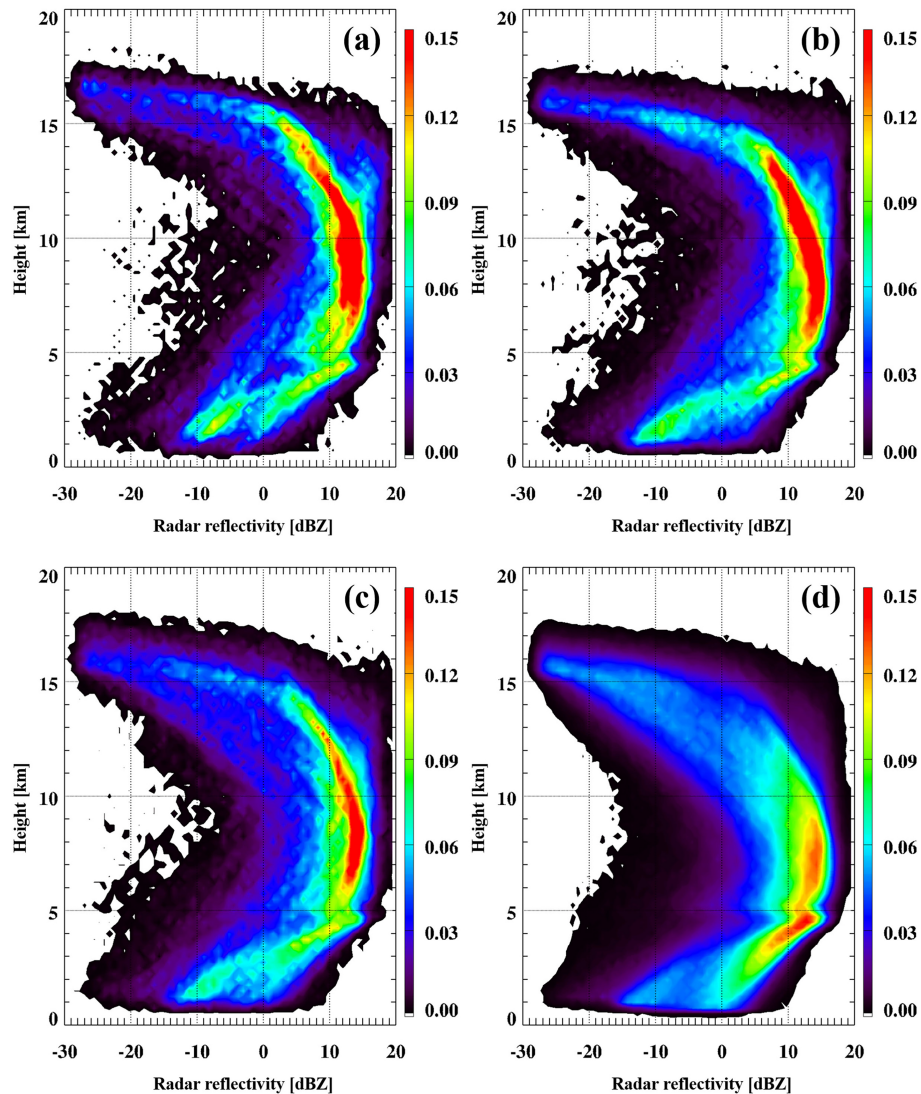


**Figure 3.** Two-dimensional histograms of radar reflectivity profiles for DCCs observed over (a) African, (b) South American, (c) western Pacific (land), and (d) western Pacific (ocean) domains. The color bars represent probability with respect to the total profiles.

## 2 Used data and methodology

### 2.1 Definition of DCC

Because DCC reaches around the tropopause level, cloud top temperature (satellite-measured infrared window channel temperature) has been often used as a criterion for determining the presence of DCC. The cloud top temperature thresholds ranging from 190 to 210 K have been used for different DCC-related study objectives (e.g., Aumann et al., 2007; Liu et al., 2007; Sohn et al., 2009). However, because the cloud top temperature criteria cannot differentiate DCCs from cirrus/anvil clouds, we use CloudSat reflectivity profiles for explicitly determining DCC, which is defined in this study to be a single-layer cloud whose depth is greater than 15 km.

### 2.2 MODIS, CloudSat, and CALIPSO measurements

MODIS is a passive imager with 36 spectral bands that cover the visible and infrared spectrum. In this study, brightness temperature at  $11\ \mu\text{m}$  ( $T_{B11}$ ) and reflectivity at  $0.645\ \mu\text{m}$  ( $Ref_{0.6}$ ) converted from MODIS-measured radiances (MYD021 products; Collection 5 version) are used to examine the characteristics of DCC top temperature and reflectivity. MODIS-derived cloud parameters such as cloud optical thickness (COT) and column-integrated effective radius ( $R_e$ ) are obtained from MYD06 products in order to analyze differences in cloud parameters between land and ocean regions in interest. All data are from MODIS Aqua products (<http://ladsweb.nascom.nasa.gov/data/search.html>).

CloudSat carries an active sensor called CPR that measures vertical profiles of reflectivity due to atmospheric hy-

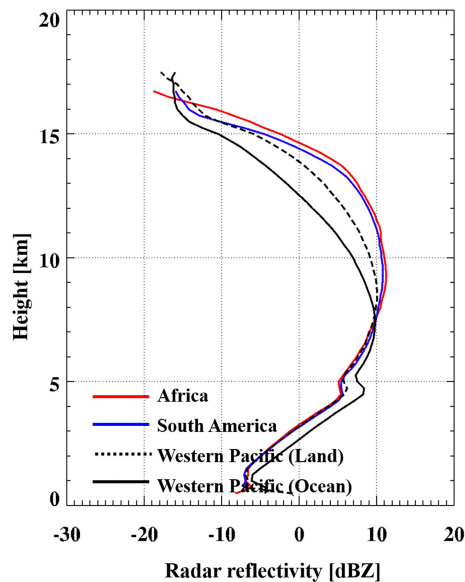


**Figure 4.** Average profiles of the radar reflectivity for the four analysis domains.

drometeors at 94 GHz. The CloudSat 2B-GEOPROF product provides radar reflectivity and cloud mask information for 125 height bins. Because a cloud mask value of 30 is considered to be a threshold ensuring cloud presence in a given layer (Mace et al., 2007), CloudSat profiles are selected for analysis if the cloud mask value is greater than 30. Beside the use of reflectivity profiles, CloudSat-retrieved cloud parameters are used. These include cloud water content and effective radius profiles obtained from CloudSat 2B-CWC-RVOD products whose pixel resolution is about 1.4 km (Wood, 2008). However, because CloudSat-derived liquid water content and liquid effective radius are erroneous as the result of miscalculation of the attenuation by liquid cloud droplets, and those problems were not yet corrected at the time of this paper's writing, only ice water content (IWC) and ice effective radius ( $R_e$ ) profile data were used in this study to examine the reflectivity difference. Because the visible extinction coefficient ( $k_{\text{ext}}$ ) is closely linked to the optical thickness and visible reflectivity observable at top of atmosphere (TOA), the  $k_{\text{ext}}$  profile is estimated as follows (e.g., Lin and Rossow, 1994):

$$k_{\text{ext}} = \frac{3}{4} \frac{Q_e}{\rho_i} \frac{\text{IWC}(z)}{R_e(z)}. \quad (1)$$

In Eq. (1), extinction efficiency ( $Q_e$ ) is considered for cloud particles to be nearly equal to 2 in the visible range, and density of ice crystals ( $\rho_i$ ) is fixed as a constant (i.e.,  $0.917 \text{ g m}^{-3}$ ), as used in CloudSat retrieval.

CALIPSO also carries an active sensor, Cloud-Aerosol Lidar with Orthogonal Polarization (CALIOP), beaming at 532 and 1064 nm wavelengths and sensitive to particles much smaller than those detectable by CloudSat. Because Cloud-

Sat misses the top portion of DCC composed of small ice crystals (Kahn et al., 2008), CALIPSO data are used for information on cloud properties above the CloudSat-detected upper boundary of the reflectivity profile. In this study, CALIPSO-derived cloud extinction coefficient at  $0.532 \mu\text{m}$  (Young and Vaughan, 2009) and ice water content (Heymsfield et al., 2005) profiles (CALIPSO L2-05kmCPro, edition 3.01) are analyzed. It is a 5 km average based on the average of 15 CALIOP FOV of 100 m laser shots.

### 2.3 Analysis domain and period

In order to examine the regionally different optical properties of DCCs, three analysis areas are selected (Fig. 1), i.e., continental Central Africa ( $20^\circ \text{N} - 20^\circ \text{S}$ ,  $0 - 40^\circ \text{E}$ ), South America ( $10^\circ \text{N} - 30^\circ \text{S}$ ,  $40 - 70^\circ \text{W}$ ), and the western Pacific ( $20^\circ \text{N} - 20^\circ \text{S}$ ,  $100 - 180^\circ \text{E}$ ). These three regions are outlined in Fig. 1, and are, respectively, represented by AF, SA, and WP. Examining the optical difference between land and ocean, the western Pacific domain, which also consists of lands such as Indonesia, Malaysia, and northern Australia, is further divided into its land area (WP-land) and ocean area (WP-ocean). Analysis is performed with data for the four January months in the 2007–2010 period. January is chosen because it is the time of year when DCCs are frequently observed over all three analysis regions.

### 2.4 Construction of collocated DCC data

Collocated DCC data are constructed over the selected four domains, using measurements from Aqua MODIS, CloudSat, and CALIPSO whose local equatorial crossing time is approximately 13:30. (Stephens et al., 2002; Parkinson, 2003; Winker et al., 2003). Due to the different MODIS scan geometry, collocation is carried out over the along-track of CloudSat by selecting the closest MODIS and CALIPSO pixels from a given CloudSat pixel. The combination of collocated CloudSat, CALIPSO, and MODIS data will provide us overall features of the physical/optical properties of DCCs, from which key factors contributing to the regional difference in DCC reflectivity can be examined.

Although the parallax correction scheme (Wang et al., 2011; Young et al., 2012) has been applied to correct the misalignment of the DCC targets caused by different viewing geometry between MODIS and CloudSat, we try to reduce possible geolocation error. This is done by taking an average of  $3 \times 3$  MODIS pixels (corresponding to about  $3 \text{ km} \times 3 \text{ km}$ ) surrounding the collocated DCC pixel as a collocated MODIS value. We further limit DCC samples to ones showing the solar zenith angle and satellite viewing zenith angle less than  $40^\circ$ .

The total numbers of pixels passing the aforementioned criteria are 980, 2295, 2455, and 23 836 for African, South American, WP-land, and WP-ocean regions, respectively. The number of DCC pixels collected for each month is given

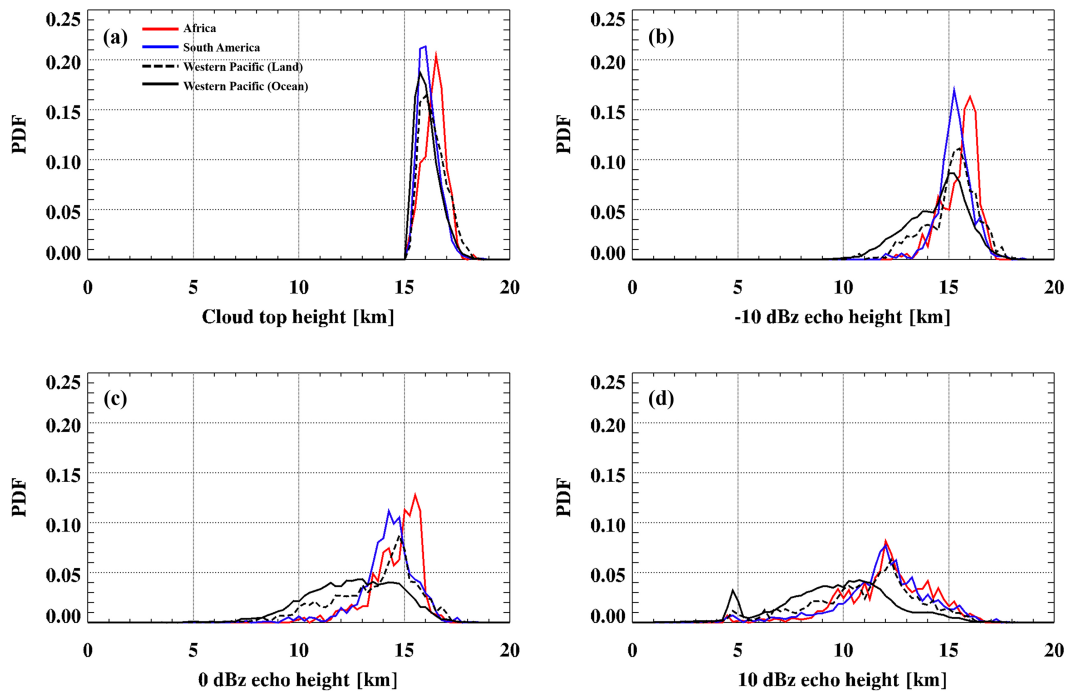


**Figure 5.** PDF distributions of (a) cloud top height; echo top height showing (b) –10, (c) 0, and (d) 10 dBz in DCC samples.

in Table 1. The selected DCC number over the African domain appears to be significantly smaller than those for others. However, considering that samples numbers are 3853, 7906, 5409, and 43996 if 14 km depth is used as a criterion for defining DCC, smaller sample size of Africa suggests that DCC clouds than deeper than 15 km are less available over Africa compared to other regions under study. Less DCC samples over Africa appear to be related to the higher surface elevation there. Since the tropopause levels should be rather homogeneous over all three analysis regions, the DCC tops should not vary much even if overshooting clouds are counted. However, cloud bottoms should have strong dependence on the surface elevation. Considering that much of tropical African land shows surface elevations above 1000 m except for the Congo Basin and that much of South American domain shows elevations well below 1000 m, the lowest DCC frequency over tropical Africa amongst three regions and lowest degree of DCC occurrence over Africa in comparison to South America are likely associated with higher topographic altitudes over tropical Africa. It may also explain why there is a drastic change in DCC samples in between 14 and 15 km of cloud depths. Nevertheless, considering that the WP domain size is about twice the size of the two continental regions, DCCs are found to be more abundant over the WP region compared to other two continental regions.

**Table 1.** The numbers of MODIS–CloudSat collocated DCC pixels over the four analysis domains. In January, only 15 days of data are available because of the battery problem of CloudSat.

	AF	SA	WP(L)	WP(O)
Jan 2007	486	859	748	8305
Jan 2008	39	495	412	5799
Jan 2009	183	696	897	5694
Jan 2010	272	245	398	4038
Total	980	2295	2455	23836

### 3 Optical properties of DCCs

#### 3.1 MODIS measurements

First, statistical distributions of selected DCC pixels are compared with one another for the four regions. In doing so, probability density functions (PDFs) of MODIS-measured  $TB_{11}$ ,  $Ref_{0.6}$ , MODIS-derived COT, and  $R_e$  are obtained and are presented in Fig. 2. PDFs for  $TB_{11}$  (Fig. 2a) show that African, South American, and WP-land regions exhibit broad peaks at colder temperatures than that for the WP-ocean region where rather broader  $TB_{11}$  distribution is noted.

Corresponding reflectivity distributions in Fig. 2b show distinctively different modes between land and ocean: African, South American, and WP-land regions exhibit a reflectivity peak around 0.95, contrasting to a mode at darker 0.89 of the reflectivity over the WP-ocean domain. It is clear

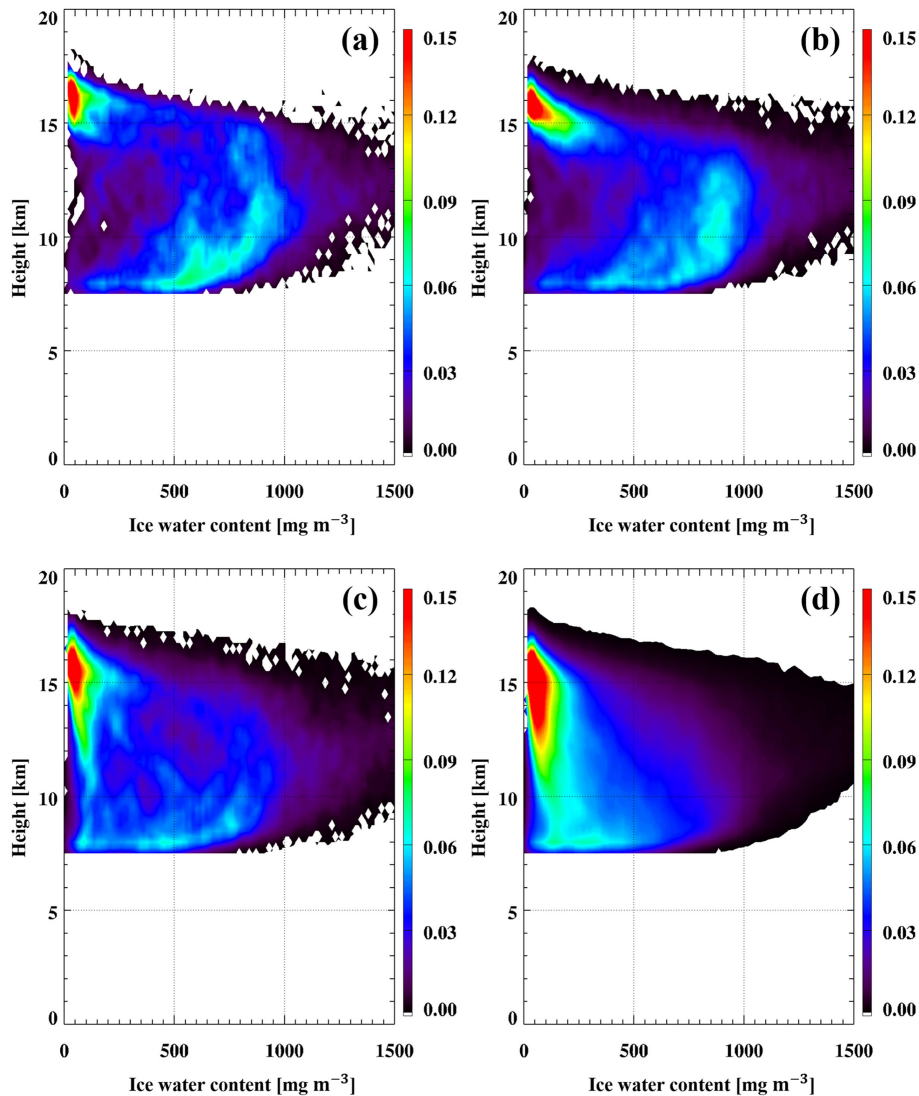


**Figure 6.** Same as Fig. 3 but for CloudSat-derived ice water content.

that DCCs found over the WP-ocean are generally darker than those found over tropical African, South American, and WP-land regions; their mean values are 0.85, 0.94, 0.93, and 0.90, respectively (Table 2). By combining these with the patterns noted in  $TB_{11}$  distributions (200.4 K vs. 196.1, 198.7, and 197.7 K), the DCCs over the WP-ocean region can be summarized as clouds having lower reflectivities with warmer cloud tops compared to other three land regions.

PDFs of MODIS-derived COT and  $R_e$  are given in Fig. 2c and d, respectively. Because the MODIS cloud algorithm only provides COT up to 100 even if clouds are thought to be optically thicker than 100, the dominant portion of PDFs should be located near COT = 100. Thus, separate plots are made for COT < 100 and for COT > 90. As shown in Fig. 2c, the majority of DCCs over the two continental regions (Africa and South America) show DCCs with COTs

higher than over the WP-ocean and WP-land. There seems to be not much discernible COTs between the WP-ocean and WP-land regions although the WP-ocean shows higher frequencies in the lower COTs. Considering that DCCs whose depths are larger than 15 km effectively remove the possible misclassification due to optically thinner anvil-type clouds, the persistent lower reflectivity over the ocean strongly suggests that DCCs found over the WP-ocean are generally darker compared to continental regions. Furthermore, based on the finding that reflectivities over the WP-land region are smaller than other two continental regions, it suffices to say that DCCs found over the western Pacific area are overall generally darker than those found in tropical continental regions.

PDF distributions of  $R_e$  of the DCCs for the four regions are given in Fig. 2d. The  $R_e$  modes are evidently differ-

**Table 2.** Mean  $\text{Ref}_{0.6}$  and  $\text{TB}_{11}$  of selected DCC pixels for the four domains.  $\text{Ref}_{0.6}$  and  $\text{TB}_{11}$  represent the MODIS reflectivity at the  $0.645 \mu\text{m}$  and MODIS brightness temperature at the  $11 \mu\text{m}$  band.

	AF		SA		WP(L)		WP(O)	
	$\text{Ref}_{0.6}$	$\text{TB}_{11}$	$\text{Ref}_{0.6}$	$\text{TB}_{11}$	$\text{Ref}_{0.6}$	$\text{TB}_{11}$	$\text{Ref}_{0.6}$	$\text{TB}_{11}$
Jan 2007	0.957	196.6	0.944	199.5	0.895	198.7	0.841	200.6
Jan 2008	0.944	197.0	0.947	197.6	0.899	196.7	0.843	200.8
Jan 2009	0.895	196.2	0.908	198.3	0.909	196.3	0.856	200.0
Jan 2010	0.940	195.1	0.936	199.0	0.854	200.1	0.845	199.8
Mean	0.939	196.1	0.929	198.7	0.900	197.7	0.846	200.4

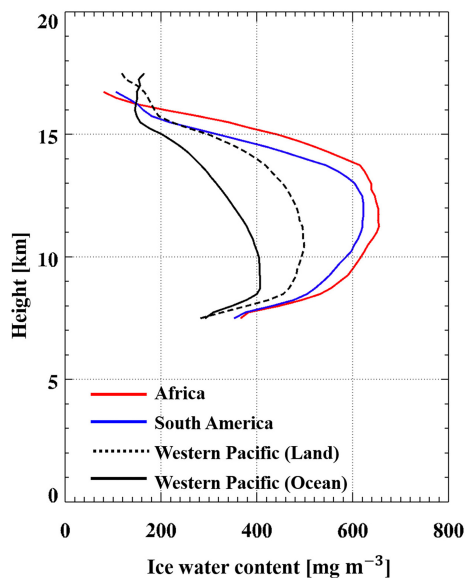


**Figure 7.** Same as Fig. 4 but for CloudSat-derived ice water content.

ent between the western Pacific and tropical land regions. It is noted that particles are relatively larger over the WP-ocean compared to other three land regions. Because backward scattering tends to decrease while forward scattering slightly increases with increasing particle size, the difference in  $R_e$  can also be considered as one of the reasons causing the regionally different DCC reflectivity over the tropical latitudes. Note that MODIS-derived cloud parameters such as COT and  $R_e$  are based purely on visible and near-infrared radiance measurements (King et al., 1997). Thus, if measured radiances are smaller, especially for the  $0.645$  and  $2.12 \mu\text{m}$  bands in the first place, smaller COT and/or larger  $R_e$  of DCCs can arise from those measurements, as was also suggested by Doelling et al. (2013). However, since MODIS-derived cloud properties cannot be independent of measured radiances themselves on focus, it should be difficult to examine measured characteristics from their derived properties. Because of this reasoning, we further use CloudSat and CALIPSO measurements to find possible causes.

## 3.2 CloudSat observations and derived cloud products

To avoid circular interpretation in the use of MODIS cloud products, we use CloudSat measurements to examine the regionally varying characteristics of tropical DCCs causing the different reflectivities.

### 3.2.1 Radar reflectivity profiles

The radar reflectivity profile is a fundamental observation of CloudSat that allows the examination of the vertical structure of DCC clouds. Two-dimensional histograms of the radar reflectivity for DCCs over Africa, South America, WP-land, and WP-ocean are given in Fig. 3. The two-dimensional distributions show similar parabolic shapes, but substantial differences exist between the WP-ocean and the three land regions. These features are more evident in the averaged profiles (Fig. 4). Large radar echoes (e.g., greater than  $10 \text{ dBZ}$ ) are more frequently observed in the  $9\text{--}12 \text{ km}$  layer of DCCs over the continental regions in comparison to the western Pacific counterpart. Moreover, maximum values of radar reflectivity for DCCs over the continental regions are located at relatively high altitudes (i.e.,  $9\text{--}12$  compared to  $7\text{--}8 \text{ km}$ ). The larger reflectivity in the higher altitudes over the tropical continental areas implies stronger convective updraft there, as in large radar echoes introduced as a proxy of strong convection (Liu et al., 2007; Luo et al., 2008, 2011). These results are consistent with the finding that typical updrafts over the African Congo region are stronger than those over the tropical Pacific and so lift larger particles into high altitudes (Liu and Zipser, 2005; Zipser et al., 2006; Liu et al., 2007). It is also of interest to note the bright band shown around  $4.5 \text{ km}$  which is due to more reflection by melting snow flakes below the melting layer at  $5 \text{ km}$  (Sassen et al., 2007). Strong attenuation is evident below the bright band altitude, probably caused by precipitating rain drops (Battaglia and Simmer, 2008).

CloudSat reflectivities of  $0$  or  $10 \text{ dBZ}$  are often used for tracing the precipitation-size particles within convective clouds (Stephens and Wood, 2007). Here, to further examine DCC structure and related convection intensity, cloud top height is determined for each sample using the radar re-

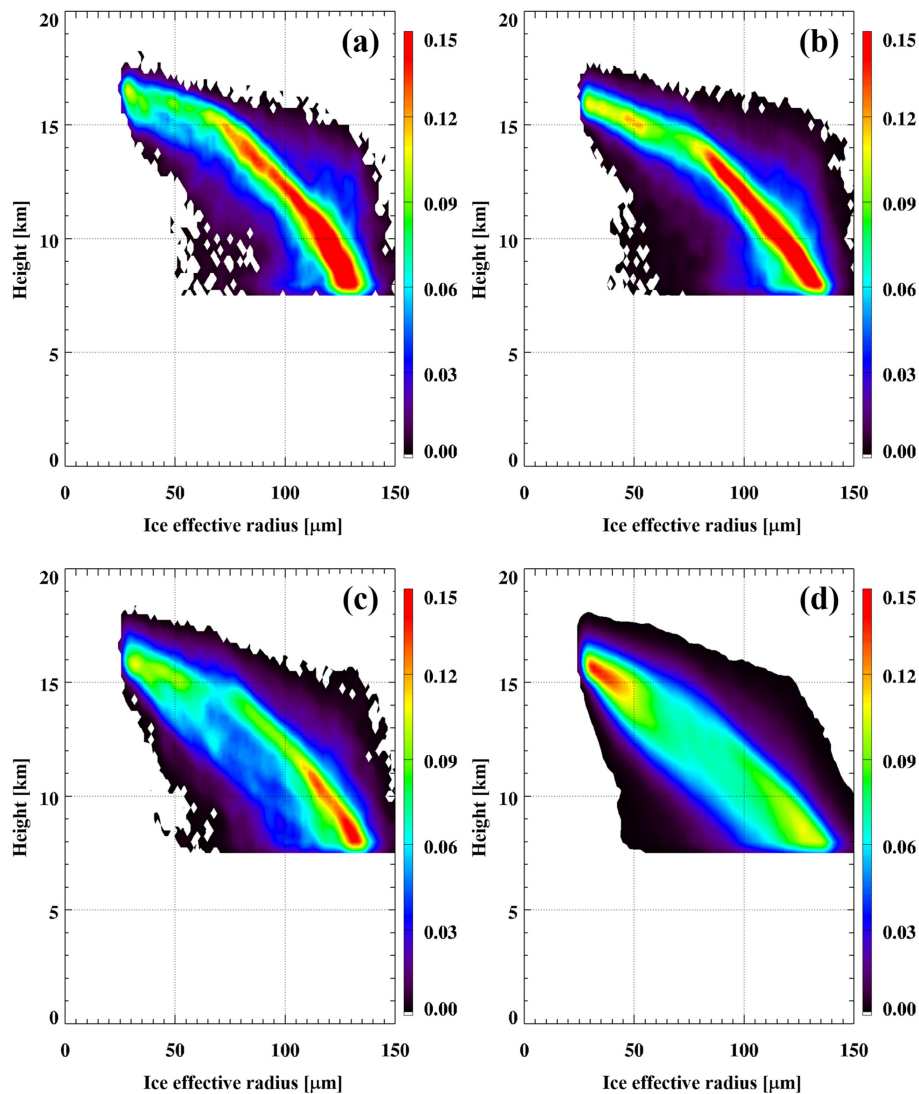


**Figure 8.** Same as Fig. 3 but for ice effective radius.

flectivity threshold of  $-28$  dBZ (Stephens et al., 2008). The highest altitudes showing radar reflectivities of  $-10$ ,  $0$ , and  $10$  dBZ (hereafter referred to as  $-10$ ,  $0$ , and  $10$  dBZ height) are also obtained. Average distributions are calculated from the obtained heights,  $-10$ ,  $0$ , and  $10$  dBZ heights, for the four analysis regions, and the results are given in Fig. 5. The mean distributions of cloud top heights for the DCCs show that the DCCs are in general slightly higher over the African region. This result is consistent with the more frequent occurrence of cold clouds over Africa (Fig. 2a).

When the distributions of the highest altitudes showing  $-10$ ,  $0$ , and  $10$  dBZ reflectivities are compared, the difference between land and ocean appears to be more pronounced regardless of the observed radar signal. The distributions of  $-10$  dBZ height seem to be similar among four regions except Africa (Fig. 5b) which shows a peak at the highest altitude around  $16$  km. Heights of  $0$  dBZ for the WP-ocean

appear to be generally lower and broader than those of the other three regions. The three land regions show a similar distribution although again Africa shows the highest echo top heights. In the case of the  $10$  dBZ height, the land regions still show a dominant peak at  $12$ – $13$  km (Fig. 5d). Thus, radar reflectivity showing a relatively larger value (here  $10$  dBZ) appears at a comparatively lower level over the WP-ocean region compared to other three land regions. Overall, the upper part of DCCs over the WP-ocean region may be less dense because the  $0$  and  $10$  dBZ heights are lower in spite of generally taller cloud compared to DCCs over tropical land regions. In other words, because the CloudSat radar reflectivity is proportional to the summed sixth-power of geometric particle size, the larger radar reflectivity in the upper part of clouds over the three land regions can be interpreted as either a larger amount of ice particles or larger sizes of ice there compared to the WP-ocean region.

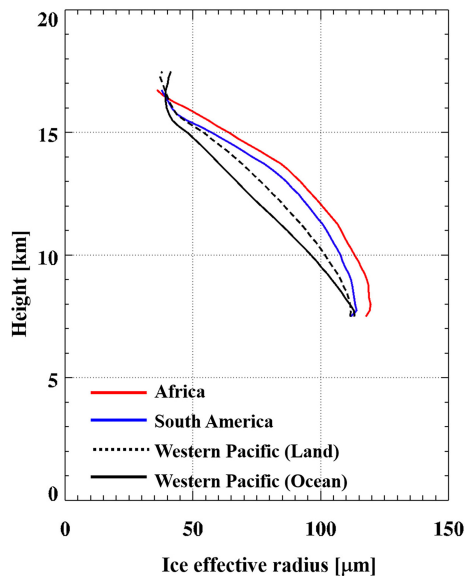


Figure 9. Same as Fig. 4 but for ice effective radius.

### 3.2.2 Profiles of ice water content

As cloud particles have a direct effect on scattering and thus reflectivity, we examine the vertical distribution of IWC of DCCs collected over the four selected regions. Two-dimensional histograms of IWC profiles are given in Fig. 6. Significant land–ocean contrast is evident in the IWC profiles as summarized in Fig. 7; a much broader IWC range is shown over the continental regions compared with the narrower IWC distribution over the WP-ocean region.

The mean profiles of IWC of DCCs over the three regions (Fig. 7) summarize the tropical land–ocean contrast discussed above. The differences in IWC between land and ocean and between the three land regions become substantial in layers below 15 km. The largest mean IWCs are shown over Africa, and their magnitudes are as much as twice those for the WP-ocean. The South American region also shows a larger amount of IWC compared to that over the WP-land and WP-ocean, although values are smaller than those over the African region. In spite of DCCs occurring over land, the WP-land region shows far smaller IWC compared to the other two land regions (i.e., Africa and South America). It appears that the WP-land region shows a profile between the WP-ocean and two continental regions. Overall, the zonal mean profile manifests that the total amount of ice water for DCCs over the WP-ocean is much smaller than those in the three land regions and that the level showing the maximum value is lower over the WP-ocean region.

### 3.2.3 Profiles of effective radius ( $R_e$ ) for ice particles

Figure 8 represents CloudSat-derived  $R_e$  profiles for DCCs over the four regions. It is noted that the narrower  $R_e$  range

with smaller particles in the upper part of DCC tends to become wider with larger particles in the layers between 10 and 15 km. It is also of interest to note that maximum occurrence levels are significantly different between the land and ocean regions; maximum occurrences for the WP-ocean are at about 15 km with particle sizes of 30–50  $\mu\text{m}$  and there exists a secondary maximum around 8–9 km. In contrast three land regions show maximum occurrences in thicker layers below 12 km with particle sizes larger than 100  $\mu\text{m}$ .

The generally increasing tendency of  $R_e$  with decreasing altitude is more evident in the averaged profiles (Fig. 9). Amongst all four regions African and South American domains show largest  $R_e$  while smallest  $R_e$  is found in the WP-ocean. The  $R_e$  in the WP-land is found to be between the WP-ocean and other two land regions. In summary,  $R_e$  for ice particles over the WP-ocean is substantially smaller than those found for the three land regions, especially below the altitude of 15 km. These CloudSat results in effective radius appear to contradict the MODIS results in Fig. 2d, which show a much smaller radius range (e.g., hardly larger than 30  $\mu\text{m}$ ) and rather larger sizes over the WP-ocean region. Furthermore, the gradual increase in particle sizes from Africa to South America and WP-land and to WP-ocean shown in the MODIS measurements appears to be opposite to the result found from the CloudSat retrievals.

### 3.2.4 Profiles of extinction coefficient ( $k_{\text{ext}}$ )

$k_{\text{ext}}$  in the visible band enables us to interpret features of cloud reflectivity at the TOA because COT is proportional to reflectivity and can be obtained by vertically integrating  $k_{\text{ext}}$  in the cloud layer. As in Eq. (1),  $k_{\text{ext}}$  in each layer can be determined from IWC and  $R_e$ , thus larger  $k_{\text{ext}}$  implies larger IWC, smaller effective radius, or both. Thus, the DCC optical properties of a smaller amount of ice water and smaller particle sizes over the WP-ocean region (or large amount of IWC and larger particles over the land regions) determined from CloudSat measurements seem to have a compensating effect of IWC and  $R_e$  on  $k_{\text{ext}}$ . The resultant  $k_{\text{ext}}$  profiles associated with ice water of DCCs are calculated and given in Fig. 10. The figure shows that the general patterns of the  $k_{\text{ext}}$  profiles are very similar to the IWC profiles in Fig. 6 although the second frequency maxima are more clear in the  $k_{\text{ext}}$  profiles. The similarity suggests that the effect from different radius between land and ocean regions and between Africa and South America appears to be minor. In other words,  $k_{\text{ext}}$  is controlled largely by the amount of IWC.

These results strongly suggest that among the four analysis domains, the reflectivity is lowest over the WP-ocean mainly because of the smaller amount of ice cloud particles there compared to the tropical continental African and South American regions and even to the land area within the western Pacific domain. Same interpretation can be applied for explaining the darker DCCs over the western Pacific in general.

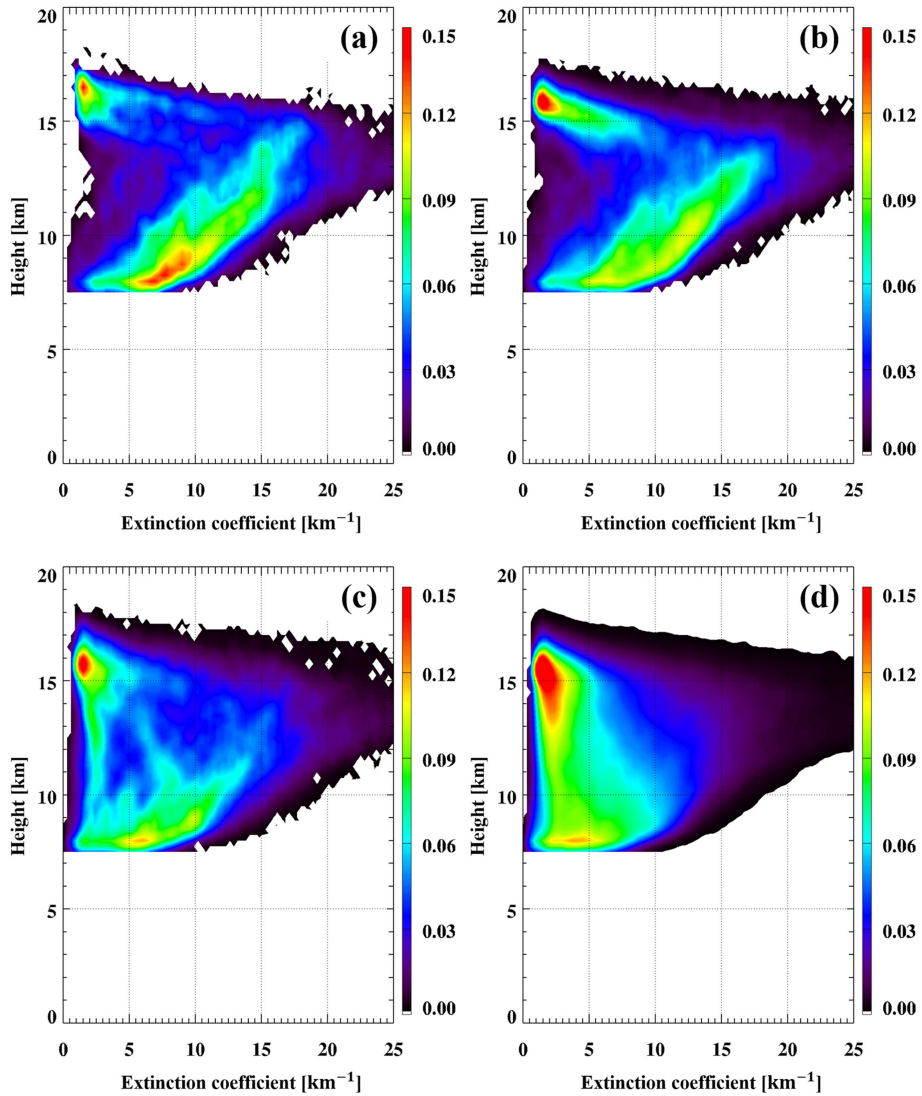


Figure 10. Same as Fig. 3 but for extinction coefficient.

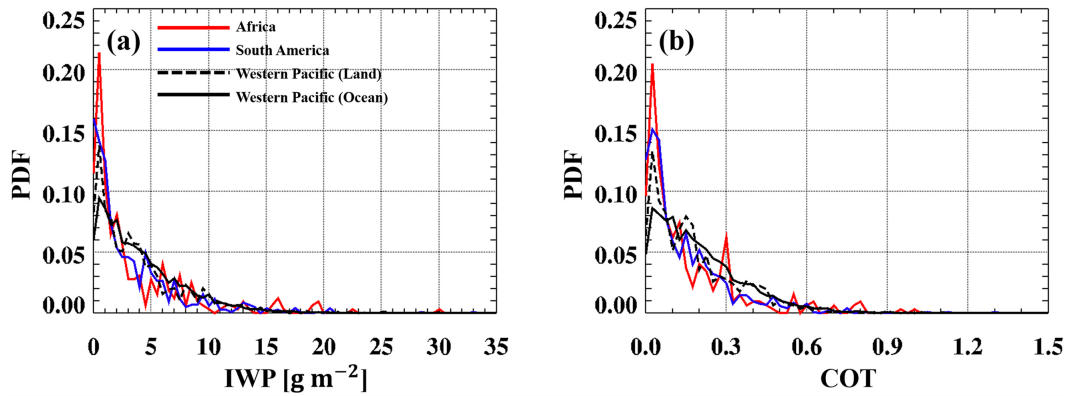


Figure 11. PDF distributions of CALIPSO-estimated (a) ice water path (IWP) and (b) cloud optical thickness (COT).

### 3.3 CALIPSO-derived ice water path (IWP) and COT

As CALIPSO uses a visible wavelength, it can observe optical properties related to small particles such as ice crystals, but observation is limited to small optical thickness because of the fast attenuation of emitted radiation. DCC heights determined from CALIPSO are relatively high, up to 2 km, compared to CloudSat-determined DCC heights, and CALIPSO observation is generally available for only a 1–3 km depth below the CALIPSO-determined cloud top in the case of convective clouds (not shown).

In order to investigate features of optical properties above the CloudSat-detected cloud top, IWP and COT are calculated by vertically integrating CALIPSO-derived layer-mean IWC and  $k_{\text{ext}}$  profiles, respectively. PDF distributions for IWP and COT are given in Fig. 11. The figure shows that all the PDF distributions are nearly similar despite substantial differences in IWP smaller than  $2 \text{ gm}^{-2}$ . The similarity of the PDFs found among the three analysis domains implies that the contribution from ice particles above the CloudSat-determined cloud top to the regionally different reflectivity is minor. Furthermore, magnitudes of IWP and COT seem too small when a majority of DCCs shows COT larger than 100 (Fig. 2). Thus, the contribution of ice particles residing in the uppermost layers of DCCs, only detected by CALIPSO measurements, to the regional difference of reflectivity should be insignificant.

## 4 Conclusions and discussion

It has been reported that DCCs over the tropical western Pacific are generally darker (i.e., lower reflectivity) compared with the reflectivities of DCCs over tropical Africa and South America. In order to examine the main cause of the lower reflectivity over the western Pacific, we examined the regional differences in cloud optical properties observed in satellite measurements of MODIS (Aqua), CloudSat, and CALIPSO, with a further separation of the western Pacific domain into its land and oceanic areas.

DCC is defined as a cloud whose depth as a single layer is greater than 15 km. From the MODIS-derived DCCs collected from the four January months of the 2007–2010 period, it was shown that the DCCs found over the western Pacific are warmer and darker than the DCCs found over the Africa, South America, and WP-land domains (200.4 K vs. 196.1, 198.7, and 197.7 K of  $\text{BT}_{11}$ ; 0.85 vs. 0.94, 0.93, and 0.90 of  $0.645 \mu\text{m}$  reflectivity). MODIS-derived COTs of DCCs showed that DCCs over the ocean area of the western Pacific are optically thinner than those over the three land regions. Consequently, DCCs over the ocean region in the western Pacific should generally be darker compared to those over African and South American regions and even to those over the land region in the western Pacific domain. It should be worthwhile to mention that DCCs over the western Pacific

land region are generally less reflective than those found over continental Africa and South America. Overall, the western Pacific DCCs are less reflective than the continental convection regions because the frequency weighted reflectivity is 0.85 over the entire western Pacific domain – compare with 0.94 and 0.93 over Africa and South America.

Compared to all land regions it is shown that both IWC and  $R_e$  of ice particles in DCCs derived from CloudSat are substantially smaller over the western Pacific. Furthermore, vertical distributions of  $k_{\text{ext}}$  calculated from IWC and  $R_e$  profiles are evidently smaller over the western Pacific, possibly leading to the lower COT and then lower TOA reflectivity there. However, considering that smaller particles contribute more to the backscattered radiation, the smaller particles there cannot explain the comparatively lower reflectivity. These results strongly suggest that darker DCCs over the western Pacific (in particular over the ocean area) are mainly caused by the smaller amount of ice water content compared to continental land regions. To be more warranted, influences of cloud life cycles are also to be counted. It is because the A-train local overpass time of 13:30 may yield samples biased toward more frequent DCC occurrence over the land.

The regional differences in DCC's optical properties noted in this study cast a cautionary warning for the use of DCCs for the solar channel calibration without taking those different factors into account when radiative transfer calculation is involved. Using a radiative transfer model under homogeneous overcast ice cloudy conditions for DCCs with  $\text{COT} = 200$  and  $R_e = 20 \mu\text{m}$ , Sohn et al. (2009) claimed that simulated radiances at the MODIS  $0.646 \mu\text{m}$  channel are in the agreement with satellite-measured radiances within an uncertainty range of  $\pm 5\%$ , which is often a calibration target for the geostationary-based solar sensor. In that paper, a criterion of  $\text{TB}_{11} < 190 \text{ K}$  was used for defining DCCs. The Sohn et al. method was implemented for examining the calibration performance of the Meteosat-8/9 Spinning Enhanced Visible Infra-Red Imager (SEVIRI)  $0.640 \mu\text{m}$  channel (Ham and Sohn, 2010), successfully demonstrating that Meteosat-8/9  $0.640 \mu\text{m}$  channels are underestimated by 6–7%.

This calibration method is particularly useful for calibrating the visible sensor not equipped with the onboard calibration system because the method only requires DCC pixels determined from measurements of window channel brightness temperature, not requiring other information from other satellites. The results obtained in this study suggest a way how the proposed calibration method using DCC samples can be improved. For instance, instead of treating selected DCCs equally to produce the same reflectivity everywhere over the tropics as in Sohn et al. (2009), radiative transfer modeling for DCCs can be done to yield less reflectivity at least over the western Pacific. It is because, as shown in Fig. 2 and Table 2, the DCCs produced over the ocean are generally less reflective than DCCs found over the continental convective regions such as Africa and South America.

*Acknowledgements.* The authors would like to thank two anonymous reviewers for providing constructive and valuable comments on how this paper could be improved. The authors are sure that this paper now carries more scientific merit; a debt of gratitude is especially owed to one reviewer who reviewed the paper with far more care than normally expected. The reviewer questioned various aspects concerning the title, data samplings, and results interpretation, as well as making suggestions for improvement, which all became indispensable in shaping the current paper. Authors also acknowledge that MODIS data/products were from NASA Goddard Space Flight Center, CloudSat data were from CloudSat Data Processing Center (<http://www.cloudsat.cira.colostate.edu/>), and CALIPSO data were from NASA EOSDIS. This study was supported by the Korea Meteorological Administration Research and Development Program under grant KMIPA 2015-1060.

Edited by: S. Buehler

## References

- Aumann, H. H., Pagano, T., and Hofstadter, M.: Observations of deep convective clouds as stable reflected light standard for climate research: AIRS evaluation, *P. Soc. Photo.-Opt. Ins.*, 6684, 668410, doi:10.1117/12.734599, 2007.
- Battaglia, A. and Simmer, C.: How does multiple scattering affect the spaceborne W-band radar measurements at ranges close to and crossing the surface-range?, *IEEE T. Geosci. Remote*, 46, 1644–1651, doi:10.1109/TGRS.2008.916085, 2008.
- Chung, E. S., Sohn, B. J., Schmetz, J., and Koenig, M.: Diurnal variation of upper tropospheric humidity and its relations to convective activities over tropical Africa, *Atmos. Chem. Phys.*, 7, 2489–2502, doi:10.5194/acp-7-2489-2007, 2007.
- Doelling, D. R., Morstad, D., Scarino, B. R., Bhatt, R., and Gopalan, A.: The characterization of deep convective clouds as an invariant calibration target and as a visible calibration technique, *IEEE T. Geosci. Remote*, 51, 1147–1159, doi:10.1109/TGRS.2012.2225066, 2013.
- Ham, S.-H. and Sohn, B. J.: Assessment of the calibration performance of satellite visible channels using cloud targets: application to Meteosat-8/9 and MTSAT-1R, *Atmos. Chem. Phys.*, 10, 11131–11149, doi:10.5194/acp-10-11131-2010, 2010.
- Heymsfield, A. J., Winker, D., and van Zadelhoff, G.-J.: Extinction-ice water content-effective radius algorithms for CALIPSO, *Geophys. Res. Lett.*, 32, L10807, doi:10.1029/2005GL022742, 2005.
- Kahn, B. H., Chahine, M. T., Stephens, G. L., Mace, G. G., Marchand, R. T., Wang, Z., Barnet, C. D., Eldering, A., Holz, R. E., Kuehn, R. E., and Vane, D. G.: Cloud type comparisons of AIRS, CloudSat, and CALIPSO cloud height and amount, *Atmos. Chem. Phys.*, 8, 1231–1248, doi:10.5194/acp-8-1231-2008, 2008.
- Kim, B. R., Ham, S.-H., Kim, D.-H., and Sohn, B. J.: Post-flight radiometric calibration of the Korean geostationary satellite COMS Meteorological Imager, *Asia-Pac. J. Atmos. Sci.*, 50, 201–210, 2014.
- King, M. D., Tsay, S.-C., Platnick, S., Wang, M., and Liou, K.-N.: Cloud retrieval algorithms for MODIS: Optical thickness, effective particle radius, and thermodynamic phase, MODIS Algorithm Theoretical Basis Document ATBD-MOD-05, NASA Goddard Space Flight Center, 83 pp., 1997.
- Lin, B. and Rossow, W. B.: Observations of cloud liquid water path over oceans: Optical and microwave remote sensing methods, *J. Geophys. Res.*, 99, 20907–20927, doi:10.1029/94JD01831, 1994.
- Liu, C. and Zipser, E. J.: Global distribution of convection penetrating the tropical tropopause, *J. Geophys. Res.*, 110, D23104, doi:10.1029/2005JD006063, 2005.
- Liu, C., Zipser, E. J., and Nesbitt, S. W.: Global distribution of tropical deep convection: different perspectives from TRMM infrared and radar data, *J. Climate*, 20, 489–503, 2007.
- Luo, Y., Zhang, R., Qian, W., Luo, Z., and Hu, X.: Intercomparison of deep convection over the Tibetan Plateau-Asian monsoon region and subtropical North America in boreal Summer using CloudSat/CALIPSO data, *J. Climate*, 24, 2164–2177, 2011.
- Luo, Z., Liu, G. Y., and Stephens, G. L.: CloudSat adding new insight into tropical penetrating convection, *Geophys. Res. Lett.*, 35, L19819, doi:10.1029/2008GL035330, 2008.
- Mace, G. G., Marchand, R., Zhang, Q., and Stephens, G.: Global hydrometeor occurrence as observed by CloudSat: Initial observations from summer 2006, *Geophys. Res. Lett.*, 34, L09808, doi:10.1029/2006GL029017, 2007.
- Nesbitt S. W., Robert., C., and Steven, A. R.: Storm morphology and rainfall characteristics of TRMM precipitation features, *Mon. Weather Rev.*, 134, 2702–2721, 2006.
- Parkinson, C. L.: Aqua: an Earth-observing satellite mission to examine water and other climate variables, *IEEE T. Geosci. Remote*, 41, 173–183, 2003.
- Sassen, K., Sergey, M., and James, C.: CloudSat spaceborne 94 GHz radar bright bands in the melting layer: An attenuation-driven upside-down lidar analog, *Geophys. Res. Lett.*, 34, L16818, doi:10.1029/2007GL030291, 2007.
- Soden, B. J. and Fu, R.: A satellite analysis of deep convection, upper-tropospheric humidity and the greenhouse effect, *J. Climate*, 8, 2333–2351, 1995.
- Sohn, B. J. and Schmetz, J.: Water vapor-induced OLR variations associated with high cloud changes over the tropics: A study from Meteosat-5 observations, *J. Climate*, 17, 1987–1996, 2004.
- Sohn, B. J., Schmetz, J., and Chung, E.-S.: Moistening processes in the tropical upper troposphere observed from Meteosat measurements, *J. Geophys. Res.*, 113, D13109, doi:10.1029/2007JD009527, 2008.
- Sohn, B. J., Ham, S.-H., and Yang, P.: Possibility of the visible-channel calibration using deep convective clouds overhooting the TTL, *J. Appl. Meteorol. Clim.*, 48, 2271–2283, 2009.
- Stephens, G. L. and Wood, N. B.: Properties of tropical convection observed by millimeter-wave radar systems, *Mon. Weather Rev.*, 135, 821–842, 2007.
- Stephens, G. L., Vane, D. G., Boain, R. J., Mace, G. G., Sassen, K., Wang, Z., Illingworth, A. J., O'Connor, E. J., Rossow, W. B., Durden, S. L., Miller, S. D., Austin, R. T., Benedetti, A., Mitrescu, C., and The CloudSat Science Team: The Cloudsat mission and the A-train., *B. Am. Meteorol. Soc.*, 83, 1771–1790, 2002.
- Stephens, G. L., Vane, D. G., Tanelli, S., Im, E., Durden, S., Rokey, M., Reinke, D., Partain, P., Mace, G. G., Austin, R., L'Ecuyer, T., Haynes, J., Lebsock, M., Suzuki, K., Waliser, D., Wu, D., Kay, J., Gettelman, A., Wang, Z., and Marchand, R.: CloudSat mission:

- Performance and early science after the first year of operation, *J. Geophys. Res.*, 113, D00A18, doi:10.1029/2008JD009982, 2008.
- Wang, C., Luo, Z. J., and Huang, X.: Parallax correction in collocating CloudSat and Moderate Resolution Imaging Spectroradiometer (MODIS) observations: Method and application to convection study, *J. Geophys. Res.*, 116, D17201, doi:10.1029/2011JD016097, 2011.
- Winker, D. M., Pelon, J., and McCormick, M. P.: The CALIPSO mission: Spaceborne lidar for observation of aerosols and clouds, Lidar Remote Sensing for Industry and Environment Monitoring III, edited by: Singh, U. N., Itabe, T., and Liu, Z., International Society for Optical Engineering, SPIE Proceedings, Vol. 4893, 1–11, 2003.
- Wood, N.: Level 2B Radar-Visible Optical Depth Cloud Water Content (2B-CWC-RVOD) process description document, Cooperative Inst. Res. Atmosphere (CIERA), Fort Collins, CO, Rep. Version 5.1, October, 2008.
- Young, A. H., Bates, J. J., and Curry, J. A.: Complementary use of passive and active remote sensing for detection of penetrating convection from CloudSat, CALIPSO, and Aqua MODIS, *J. Geophys. Res.*, 117, D13205, doi:10.1029/2011JD016749, 2012.
- Young, S. A. and Vaughan, M. A.: The retrieval of profiles of particulate extinction from Cloud-Aerosol Lidar Infrared Pathfinder Satellite Observations (CALIPSO) Data: Algorithm Description, *J. Atmos. Ocean. Tech.*, 26, 1105–1119, 2009.
- Zipser, E. J., Cecil, D., Liu, C., Nesbitt, S., and Yorty, D.: Where are the most intense thunderstorms on earth?, *B. Am. Meteorol. Soc.*, 87, 1057–1071, 2006.